Atmos. Chem. Phys. Discuss., 12, 29025–29067, 2012
www.atmos-chem-phys-discuss.net/12/29025/2012/
doi:10.5194/acpd-12-29025-2012

Atmospheric Chemistry and Physics Discussions

Characterization of photochemical pollution at different elevations in mountainous areas in Hong Kong

H. Guo[1], Z. H. Ling[1], K. Cheung[1], F. Jiang[2], D. W. Wang[1], I. J. Simpson[3], T. J. Wang[4], X. M. Wang[5], S. M. Saunders[6], and D. R. Blake[3]

[1]Air Quality Studies, Department of Civil and Environmental Engineering, the Hong Kong Polytechnic University, Hong Kong, China
[2]International Institute for Earth System Science, Nanjing University, Nanjing, China
[3]Department of Chemistry, University of California at Irvine, California, USA
[4]School of Atmospheric Sciences, Nanjing University, Nanjing, China
[5]Guangzhou Institute of Geochemistry, Chinese Academy of Sciences, Guangzhou, China
[6]School of Biomedical, Biomolecular and Chemical Sciences, University of Western Australia, Perth, Australia

Received: 24 August 2012 – Accepted: 26 October 2012 – Published: 12 November 2012

Correspondence to: H. Guo (ceguohai@polyu.edu.hk) and
Z. H. Ling (patrick.ling@connect.polyu.hk)

Published by Copernicus Publications on behalf of the European Geosciences Union.

Abstract

To advance our understanding on the factors that affect photochemical pollution at different elevations in mountainous areas, concurrent systematic field measurements (September to November 2010) were conducted at a mountain site and at an urban site at the foot of the mountain in Hong Kong. The mixing ratios of air pollutants were greater at the foot of the mountain (i.e. Tsuen Wan urban site, TW) than near the summit (i.e. Tai Mao Shan mountain site, TMS), except for ozone. In total, only 1 O_3 episode day was observed at TW, whereas 21 O_3 episode days were observed at TMS. The discrepancy of O_3 at the two sites was attributed to the mixed effects of NO titration, vertical meteorological conditions, regional transport and mesoscale circulations. The lower NO levels at TMS and the smaller differences of "oxidant" O_x (O_3 + NO_2) than O_3 between the two sites suggested that variations of O_3 at the two sites were partly attributed to different degree of NO titration. In addition, analysis of vertical structure of meteorological variables revealed that the inversion layer at the range of altitudes of 500–1000 m might be another factor that caused the high O_3 levels at TMS. Furthermore, analyses of the wind fields and the levels of air pollutants in different air flows indicated that high O_3 concentrations at TMS were somewhat influenced by regional air masses from the highly polluted Pearl River Delta (PRD) region. In particular, the analysis of diurnal profiles and correlations of gaseous pollutants suggested influence of mesoscale circulations which was further confirmed using the Master Chemical Mechanism moving box model (Mbox) and the Weather Research and Forecasting (WRF) model. By investigating the correlations of observed O_3 and NO_x^*, as well as the ratios of VOC/NO_x, it was concluded that photochemical O_3 formation was VOC-sensitive or both NO_x and VOC-sensitive at TMS, while it was VOC-sensitive at TW.

ACPD
12, 29025–29067, 2012

1 Introduction

Distinguished from surface measurements and aircraft observations, studies conducted in mountain areas often provide information on the regional background concentrations of air pollutants, the influence of regional transport and mesoscale circulations, the photochemistry of biogenic volatile organic compounds (BVOCs), and the influence of meteorological factors on ozone (O_3) chemistry (Pochanart et al., 2003; Zellweger et al., 2003; Gao et al., 2005; Wang et al., 2006; Fu et al., 2010). The characteristics of O_3 in mountainous areas have been investigated in different locations in recent years (e.g. Evtyugina et al., 2009; Scott and Ahmet, 2009; Crowley et al., 2010). For example, Burley and Bytnerowicz (2011) investigated the O_3 distribution at White Mountains (1237–4342 m) in California and concluded that high O_3 concentrations were correlated with slow-moving back-trajectories which had spent more time inland and less time offshore. Monteiro et al. (2012) analyzed a high O_3 episode by a statistical technique and a modeling approach at a mountain site (1086 m) in the Mediterranean region, and reported that transport of O_3 and its precursors by local mountain breezes and sea-breeze circulation was mainly responsible for the high O_3 concentrations. Turnipseed et al. (2004) simulated the mesoscale atmospheric flow conditions influenced by regional topography in the Niwot Ridge Ameriflux site within the Rocky Mountains (3050 m), and significant influence of mesoscale winds was found under the strong synoptic westerly winds. Ou Yang et al. (2012) investigated the seasonal and diurnal variations of O_3 at a high-altitude mountain site (2862 m) in central Taiwan and concluded that the springtime maximum O_3 concentration was most likely caused by the long-range transport of air masses from Southeast Asia.

In mainland China, limited studies have been undertaken to investigate the characteristics of O_3 pollution in mountainous areas (e.g. Gao et al., 2005; Wang et al., 2006; Li et al., 2008; Xue et al., 2011). Gao et al. (2005) reported measurements of O_3 and CO at the summit of Mt. Tai (1534 m) and suggested that air masses from the North China Plains or the re-circulation over the Shandong Peninsula had significant

ACPD
12, 29025–29067, 2012

influence on air pollutants. Li et al. (2008) investigated the impact of chemical production and transport on summer diurnal O_3 behavior at a mountainous site in North China Plain. They suggested that in-situ chemistry accounted for most of the O_3 increment from morning to mid-afternoon. Wang et al. (2006) and Xue et al. (2011) studied the origin of surface O_3 and reactive nitrogen speciation at Mt. Waliguan (3816 m) in western China, and indicated that high O_3 events were mostly derived from the downward transport of the upper tropospheric air rather than anthropogenic pollution. Nonetheless, all of these studies were carried out only at mountain sites in northern/western China.

Hong Kong and the rest of Pearl River Delta (PRD) region are situated along the coast of southern China. The rapid economic development has caused elevated levels of air pollution in this region (Huang et al., 2006; Guo et al., 2009). Owning to its critical role in the atmospheric oxidizing capacity, human health and vegetation (NRC, 1991; PORG, 1997; IPCC, 2007), photochemical O_3 has been studied in Hong Kong and the PRD region for the past two decades (Chan et al., 1998a,b; Wang et al., 2003; Ding et al., 2004; Zhang et al., 2007; Guo et al., 2009). Though these studies help us better understand the O_3 pollution in the PRD region, they were conducted at low-elevation urban and rural sites (< 50 m).

In this study, comprehensive and systematic measurements of major air pollutants were conducted simultaneously both near the summit and at the foot of Mt. Tai Mo Shan in Hong Kong. The characteristics of air pollutants and the causes of variations of air pollutants at the two sites were investigated; the relationships between the two sites and the influence of mesoscale circulations were explored by integrated data analysis and different models, and the relationships of O_3-precursors at the two different sites were further evaluated. To our best knowledge, this is the first attempt to conduct these concurrent measurements and comprehensive analysis of air pollutants in this region.

ACPD
12, 29025–29067, 2012

2 Methodology

2.1 Site description

In this study, field measurements were carried out simultaneously at different elevations at the highest mountain in Hong Kong, Mt. Tai Mo Shan (Mt. TMS) (Fig. 1). Sampling was conducted from 6 September to 29 November, 2010, when high O_3 mixing ratios were frequently observed in this season (So and Wang, 2003; Wang et al., 2005). The Hong Kong Environmental Protection Department (HKEPD) air quality monitoring station at Tsuen Wan (TW) – the closest HKEPD monitoring station at the foot of Mt. TMS – was selected as the measurement site at the foot of the mountain (22.373° N, 114.112° E, elevation of 10 m). TW is a mixed residential, commercial and light industrial area in the New Territories in Hong Kong. The site is adjacent to a main traffic road and surrounded by residential and industrial blocks. The high-elevation site (TMS) was set up on the rooftop of a building at Mt. TMS (22.405° N, 114.118° E) at an elevation of 640 m. The TW and TMS sites are separated by a straight distance of about 5 km and an elevation of 630 m.

Mt. TMS is surrounded by 1440 ha of natural territory and borders with Tai Po Kau Nature Reserve to the east, Shing Mun Country Park to the south, Route Twisk highway and Tai Lam Country Park to the west, and the old valley of the Lam Tsuen to the north (AFCD, 2008). Surrounding the foot of the mountain are urban centers with a population of 2.23 million, including Tsuen Wan, Sha Tin, Tuen Mun and Yuen Long areas. The straight distances between the mountain summit and the urban centers at the foot are about 5–10 km. Further to the south are the urban centers of the partial New Territory, Kowloon peninsula, Hong Kong Island and the South China Sea. To the southwest are the newly-developed residential area of Tung Chung, the Hong Kong international airport and the South China Sea. Because of its unique topography, mesoscale circulations, i.e. mountain-valley breezes and sea-land breezes, are often observed at Mt. TMS, which would enhance the interaction of polluted urban air and the mountain air.

ACPD
12, 29025–29067, 2012

2.2 Measurement techniques

2.2.1 Continuous measurements of O_3, CO, SO_2 and NO_x

Hourly data of O_3, CO, SO_2, NO-NO_2-NO_x and meteorological parameters at TW was obtained from the HKEPD (http://epic.epd.gov.hk/ca/uid/airdata). Detailed information about the measurements, quality assurance and control protocols can be found in the HKEPD report (HKEPD, 2012). At TMS, sampling instruments were installed in a room of a building and ambient air samples were drawn through a 5 m long perfluoroalkoxy (PFA) Teflon tube (OD: 12.7 mm; ID: 9.6 mm). The inlet of the sampling tube was located 2 m above the rooftop of the building and was connected to a PFA manifold with a bypass pump drawing air at a rate of 5 L min^{-1} into the intakes of the analyzers for O_3, CO, SO_2 and NO-NO_2-NO_x.

O_3 was measured using a commercial UV photometric instrument (Advanced Pollution Instrumentation (API), model 400E) with a detection limit of 0.6 ppbv. This analyzer was calibrated by a transfer standard (TEI 49PS) prior to the field studies. Sulfur dioxide was measured by a pulsed UV fluorescence (API, model 100E) with a detection limit of 0.4 ppbv and 2-σ precision of 0.5 % for ambient levels of 50 ppbv (2-min average). Carbon monoxide was measured with a gas filter correlation, nondispersive infrared analyzer (API, Model 300E) with a heated catalytic scrubber to convert CO to CO_2 for baseline determination. Zeroing was conducted every 2 h for 12 min. The 2-min data at the end of each zeroing were taken as the baseline. The detection limit was 30 ppbv for a 2 min average. The 2 s precision was about 1 % for a CO level of 500 ppbv (2 min average) and the overall uncertainty was estimated to be 10 %. Oxides of nitrogen were detected using a commercial chemiluminescence with an internal molybdenum converter (API, Model 200E) and a detection limit of 0.4 ppbv. The analyzers were calibrated daily by injecting scrubbed ambient air (TEI, Model 111) and a span gas mixture. A NIST-traceable standard (Scott-Marrin, Inc.) containing 156.5 ppmv CO (±2 %), 15.64 ppmv SO_2 (±2 %), and 15.55 ppmv NO (±2 %) was diluted using a dynamic calibrator (Environics, Inc., Model 6100). For the O_3, SO_2, CO and NO-NO_2-NO_x

ACPD
12, 29025–29067, 2012

analyzers, a data logger (Environmental Systems Corporation, Model 8832) was used to control the calibrations and to collect data, which were averaged to 1-min intervals.

Meteorological parameters, including temperature, solar radiation, relative humidity, wind speed and wind direction, were monitored by a weather station (Vantage Pro TM & Vantage Pro 2 plus TM Weather Stations, Davis Instruments).

2.2.2 Sampling and analysis of VOCs

Concurrent VOC samples were collected on selected non-O_3 episode (i.e. 28 September, 2, 8, 14, 18–19, 27–28 October, and 20–21 November) and O_3 episode days (i.e. 23–24, 29–31 October, 1–3, 9 and 19 November) at both sites. The potentially high O_3 episode days were selected based on weather prediction and meteorological data analysis, and were generally related to stronger solar radiation, lower wind speeds, and less vertical dilution of air pollution compared to non-O_3 episode days. These O_3 episode and non-O_3 episode days were later on confirmed by the observed O_3 mixing ratios. Ambient VOC samples were collected using cleaned and evacuated 2-l electro-polished stainless steel canisters. The canisters were prepared and delivered to Hong Kong by the Rowland/Blake group at University of California, Irvine (UCI). A flow-controlling device was used to collect 1-h integrated samples. During non-O_3 episode days, hourly VOC samples were collected at 2-h intervals from 07:00 a.m. to 07:00 p.m. per day at both sites. For O_3 episode days, hourly samples were consecutively collected from 09:00 a.m. to 04:00 p.m., with additional samples collected at 06:00 p.m., 09:00 p.m., midnight, 03:00 a.m. and 07:00 a.m. Due to logistic issues, 19 additional samples were collected at TMS, and one additional sample was taken at TW. Totally, 201 and 183 VOC samples were collected at TMS and TW, respectively.

Before sampling, all canisters were cleaned at least five times by repeatedly filling and evacuating with humidified pure nitrogen gas (N_2). To test for any contamination in the canister, the evacuated canister was filled with pure N_2, stored for at least 24 h, then checked by the same VOC analytical methods to ensure that all the target compounds were not found or were under the method detection limit (MDL). In addition,

ACPD
12, 29025–29067, 2012

duplicate samples were regularly collected to check the precision and reliability of the sampling and analytical methods. After sampling, the VOC samples were returned to the laboratory at UCI for chemical analysis. The analytical system, which is fully described in Simpson et al. (2010), uses multicolumn gas chromatography (GC) with five column-detector combinations. The oven parameters employed for each GC can be found in Colman et al. (2001).

VOCs were identified by their retention times and their mass spectra. The quantification of target VOCs was accomplished using multi-point external calibration curves, a combination of National Bureau of Standards, Scott Specialty Gases (absolute accuracy estimated to be within ±5 %) and UCI made standards. The detection limit, measurement precision and accuracy for each VOC varies by compound class and is listed in Simpson et al. (2010). Generally, alkanes, alkenes and aromatics have a detection limit of 3 pptv, a precision of 3 %, and an accuracy of 5 %.

2.3 WRF simulation

The Weather Research and Forecasting (WRF) model is a next-generation mesoscale numerical weather prediction system designed to serve both operational forecasting and atmospheric research needs (Skamarock and Klemp, 2008). It is suitable for use in a broad spectrum of applications across scales ranging from meters to thousands of kilometers. Simulations and real-time forecasting tests have indicated that the WRF model has a good performance for weather forecasts, and has broad application prospects (Steven et al., 2004; Done et al., 2004). For details, please refer to Guo et al. (2009).

As mountain-valley breezes are small scale weather phenomena caused by thermal forcing, and there is a complex terrain in Hong Kong (AFCD, 2008), considerably high model resolution is needed to capture these breezes. In this study, the mountain-valley breezes were simulated using a domain system of five nested grids (36, 12, 4, 1.333, and 0.444 km). The domain with finest resolution (0.444 km grid) covers the Hong Kong region. In the vertical scale, there were 31 sigma levels for all five domains, with the

ACPD
12, 29025–29067, 2012

model top fixed at 100 hPa. For physical processes, the WRF single-moment 3-class microphysics scheme, RRTM long wave radiation scheme, Goddard short wave radiation scheme, MM5 similarity surface layer, Noah land surface model coupled with urban canopy model, and Yonsei planetary boundary layer scheme were applied for all domains. The Grell-Devenyi ensemble cumulus parameterization scheme was applied for the outer three domains, while there was no cumulus parameterization scheme in the inner two domains. In addition, the distribution of urban land cover was replaced using the latest data downloaded from http://webmap.ornl.gov.

2.4 Master chemical mechanism box (Mbox) model simulation

In this study, a photochemical box model (PBM) implementing the most up-to-date version of near-explicit photochemical mechanism, the Master Chemical Mechanism version 3.2 (MCM3.2) has been applied to simulated the O_3 pollution at the two sites (Lam et al., 2012). MCMv3.2 was employed to describe the photochemical degradation in this study, including 143 VOCs in 16 500 reactions (Jenkin et al., 1997, 2003; Saunders et al., 2003; Bloss et al., 2005). The mechanism is accessible via the website: http://mcm.leeds.ac.uk/MCM. Three model scenarios were considered in this study: (1) Stationary photochemical box in TW: in this scenario, the monitoring station at TW was assumed to be the centre of the box model and the concentrations of the targeted species were homogenous throughout the box. Hence, the model in scenario 1 was constrained with TW data only; (2) Stationary photochemical box in TMS: similar to scenario 1, monitoring station at TMS was assumed to be the centre of the box model and the model was constrained only with TMS data; (3) Moving box (Mbox): this scenario was an over simplified mountain-valley breezes phenomenon with the grid sits between TW and TMS monitoring stations and an air parcel was moving on an idealised trajectory. In the daytime (08:00–17:00 LT), TW was assumed to be the center of the box model and the air parcel from this site followed the valley breezes entering the grid simultaneously; when at dusk, TMS was assumed to be the center and the

ACPD
12, 29025–29067, 2012

air parcel was carried back down by the mountain breezes into the grid until the next morning (18:00–07:00 LT).

3 Results and discussion

3.1 Overall observation results

3.1.1 Levels of trace gases and O_3 episodes

Table 1 summarizes the statistics of trace gases during the sampling period. In general, the mixing ratios of air pollutants were greater at TW than TMS, whereas the secondary pollutant O_3 was greater at TMS than TW. The average concentrations of NO_x, CO and SO_2 at TMS were 10.7 ± 0.3 ppbv, 436 ± 7 ppbv and 4.1 ± 0.1 ppbv, which were 0.19, 0.85 and 0.67 times those measured at TW, respectively. On the other hand, the mean O_3 concentration was 55 ± 1 ppbv at TMS, 2.5 times that of TW. The O_3 levels measured at TMS were comparable to those measured at other continental mountain sites in the Northern Hemisphere, i.e. Mt. Tai (1534 m, Gao et al., 2005) and Mt. Waliguan (3816 m, Wang et al., 2006; Xue et al., 2011) in China, and Mt. Jungfraujoch in Switzerland (3580 m, Zellweger et al., 2003), all in the range of 49–59 ppbv despite different latitudes and sampling time. As expected, the O_3 level at TMS was higher than Mt. Mondy (39 ppbv, 2006 m, Pochanart et al., 2003) in Siberia, a remote background site in East Asia.

To gain further information on the O_3 pollution at the two sites, the frequency of O_3 episode days was investigated. An O_3 episode day is defined when the peak one-hour average O_3 mixing ratio exceeds 100 ppbv (i.e. China's Grade II Standard). At the urban TW site, only 1 O_3 episode day (19 September, concentration = 116 ppbv) and 3 near-O_3 episode days (i.e. the peak hourly O_3 mixing ratio between 80–100 ppbv, or China's Grade I Standard) were observed. At the TMS site, the maximum hourly average O_3 mixing ratio reached 163 ppbv. 21 O_3 episode days (i.e. 8, 19–20 September, 23–24,

ACPD
12, 29025–29067, 2012

29– 31 October, 1–3, 8–9, 11, 17–19, 22–23, 26–27 November) were found during the sampling period.

3.1.2 Diurnal variation

Figure 2a,b shows the diurnal variations of mean O_3, NO_x, CO, SO_2 and surface winds at TMS and TW, respectively. TMS and TW had similar diurnal patterns of O_3, experiencing O_3 maxima in the afternoon and minimum at night and in the morning. However, the average daily maximum O_3 mixing ratio at TMS (70 ± 6 ppbv, 15:00 LT) was higher ($p < 0.05$) than that observed at TW (35 ± 4 ppbv, 14:00 LT). At TMS, O_3 exhibited relatively stable concentrations from midnight to the early morning, a decrease at sunrise, a minimum at about 10:00 local time (LT), a daytime buildup to a broad maximum value at about 15:00 LT, and a slow decrease until midnight, with an average diurnal difference of 16 ppbv. The slow nighttime decay of O_3 at TMS might be attributed to the limited NO titration and the reduced boundary layer mixing height. Indeed, the boundary layer height was approximately 2 km in the daytime and reduced to about 1 km at night in Hong Kong (Guo et al., 2012). At TW, a trough of O_3 was observed in the morning at about 07:00 LT, likely due to the high concentrations of NO which titrated part of the O_3 (to be discussed in detail in Sect. 3.2.2).

The diurnal variation of NO_x at the TW site showed a typical urban profile, i.e. bimodal structure. The first peak appeared in the early morning (07:00–09:00 LT) while the second peak was at about 18:00–19:00 LT, coincident with the traffic pattern of Hong Kong. On the other hand, a broad NO_x peak with a delay (compared to TW) was observed at TMS. The peak NO_x value (15.3 ± 2.2 ppbv) at TMS was much lower ($p < 0.01$) than that at TW (84.5 ± 8.1 ppbv). In addition, the diurnal profiles of SO_2 and CO were similar at TMS, with a small and broad peak in the afternoon, which might be indicative of the influence of regional transport (Guo et al., 2009; Jiang et al., 2010) and/or mesoscale circulations (Parrish et al., 1993; Gao et al., 2005; Wang et al., 2006).

ACPD
12, 29025–29067, 2012

3.2 Which factors are responsible for the discrepancy of O_3 pollution observed at TMS and TW?

While comparable solar radiation was found at the two sites ($p > 0.1$, with the average value of 275 ± 114 and $270 \pm 105\,W/m^2$ at TMS and TW), higher temperature, lower relative humidity and wind speed, which are conducive for photochemical O_3 formation (Wang et al., 2003; Jiang et al., 2008; Guo et al., 2009), were found at the urban TW site (Fig. 2a, b). Nonetheless, the O_3 concentrations at TW were much lower than TMS. The difference of the mean O_3 levels between the two sites during the sampling period was 33 ppbv (Table 1), while hourly differences reached up to 122 ppbv. As the two sites are separated by a distance of about 5 km and an elevation of 630 m, the factors that could cause the discrepancy of O_3 levels observed at the two sites are discussed in the following sections.

3.2.1 Degree of photochemical reactions

Comparing the levels of precursors is a useful tool to investigate the degree of photochemical reactions at two different sites (Sillman, 1999; Jenkin and Clemitshaw, 2000). Figure 3a shows the mean mixing ratios of different VOC groups at the two sites. The VOC species were classified into six functional types, i.e., R-AROM group (including xylenes, toluene, trimethylbenzenes and ethylbenzene), R-OLE (reactive olefins, comprising all olefins except ethene), $C \geq 4$ (including alkanes with four or more carbons), LRHC (low reactive hydrocarbon carbons, comprising ethane, propane, ethyne and benzene), ETHE (ethene) and BVOC (including isoprene, α/β-pinene and limonene). During the sampling period, the VOC levels were considerably lower at TMS than TW ($p < 0.01$), which is consistent with other O_3 precursors, i.e. NO_x and CO (Table 1).

In addition, the levels of hydroxyl radical (OH radical) at the two sites were evaluated. Figure 3b presents the calculated and model-simulated mixing ratios of OH radical at TMS and TW. The calculated mixing ratios of OH radical can be attained through the relationship between isoprene (ISOP) and its oxidation products, namely methacrolein

ACPD
12, 29025–29067, 2012

(MAC) and methyl vinyl ketone (MVK), which is presented by the following equations (Eqs. 1–5, details in Liu et al., 2009),

$$\mathrm{ISOP} + \mathrm{OH} \rightarrow 0.63\mathrm{HCHO} + 0.32\mathrm{MVK} + 0.23\mathrm{MAC} \quad k_1 = 1.0 \times 10^{-10}\,\mathrm{cm}^{-3}\,\mathrm{s}^{-1} \tag{1}$$

$$\mathrm{MAC} + \mathrm{OH} \rightarrow \mathrm{products} \quad k_2 = 3.3 \times 10^{-11}\,\mathrm{cm}^{-3}\,\mathrm{s}^{-1} \tag{2}$$

$$\mathrm{MVK} + \mathrm{OH} \rightarrow \mathrm{products} \quad k_3 = 1.9 \times 10^{-11}\,\mathrm{cm}^{-3}\,\mathrm{s}^{-1} \tag{3}$$

$$\frac{[\mathrm{MAC}]}{[\mathrm{ISOP}]} = \frac{0.23k_1}{(k_2 - k_1)}\left(1 - e^{(k_1 - k_2)[\mathrm{OH}]_{\mathrm{avg}}t}\right) \tag{4}$$

$$\frac{[\mathrm{MVK}]}{[\mathrm{ISOP}]} = \frac{0.32k_1}{(k_3 - k_1)}\left(1 - e^{(k_1 - k_3)[\mathrm{OH}]_{\mathrm{avg}}t}\right) \tag{5}$$

where [MAC], [ISOP] and [MVK] were the measured values for MAC, isoprene and MVK, and t is the processing time. The mixing ratios of OH radical were further simulated by Master Chemical Mechanism (MCM) model (details in Lam et al., 2012). The average mixing ratios of OH radical were comparable ($p > 0.05$) at the two sites, with 1.54 ± 0.24 molecule cm^{-3} (1.81 ± 0.50 molecule cm^{-3} from model simulation) at TMS and 1.72 ± 0.20 molecule cm^{-3} (2.17 ± 0.50 molecule cm^{-3} for model simulation) at TW. By considering the factor of fractional conversion which represented the relative importance of photolysis reactions on OH radical formation in the atmosphere (Jenkin et al., 2000; Atkinson et al., 1997), the mean fraction conversion indexes at TMS (0.17 ± 0.03) were lower than that at TW (0.23 ± 0.04, $p < 0.05$). Based on the aforementioned analyses, it could be concluded that photochemical reactions at TMS were not stronger than TW; therefore, the higher O_3 levels observed at TMS compared to TW were not induced by the different degrees of photochemical reactions at the two sites.

3.2.2 Influence of NO titration

The feature of higher O_3 at the higher elevation site (TMS) than the ground-level site (TW) is somewhat in line with the vertical profiles of O_3 observed in Hong Kong and

ACPD
12, 29025–29067, 2012

other locations (e.g. Wang et al., 2001; Chen et al., 2002; Tseng et al., 2009; Ma et al., 2011). Wang et al. (2001) showed that O_3 generally increased with elevation above surface and had a modest peak between 550 and 650 m at the subtropical Cape D'Aguilar site in Hong Kong in October and November, 2001. In addition, Chen et al. (2002) and Tseng et al. (2009) reported that high O_3 concentrations appeared at the height of 500–600 m and decreased rapidly towards the ground during daytime in central Taiwan. Both studies suggested that high O_3 concentrations in the higher elevations were partially attributed to the limited NO titrations, due to the lower levels of NO at higher elevations. In this study, the average NO mixing ratio at the mountain site TMS was 3.5 ± 0.1 ppbv, compared to 28 ± 1 ppbv at TW, suggesting that the higher O_3 mixing ratios at TMS were likely attributed to the limited NO titration ($O_3 + NO = NO_2 + O_2$). The NO titration is a main process of loss for O_3, which can convert NO to NO_2 rapidly (Tang et al., 2012). In order to investigate the titration effect, the concentrations of "oxidant" O_x (the concentration of $O_3 + NO_2$) were calculated at the two sites (Jenkin et al., 2000; Chen et al., 2002; Jiang et al., 2010). The mean O_x mixing ratio was 47 ± 1 ppbv at TW, close to the value (58 ± 1 ppbv) found at TMS (Table 1), confirming lower degree of NO titration at the TMS site.

3.2.3 Influence of vertical meteorological conditions

Besides NO titration, vertical structure of meteorological variables is an important factor that could influence the O_3 levels at different elevations (Lin et al., 2007; Ma et al., 2011). Therefore, we investigated the vertical profiles of meteorological conditions, such as temperature and relative humidity in Hong Kong at the selected 40 days, including 21 O_3 episode days and selected 19 non-O_3 episode days before/after the O_3 episode days. Two cases (23 and 27 October) were presented here as examples (Fig. 2c). The vertical profile of meteorological data for Hong Kong was downloaded from the Department of Atmospheric Science, College of Engineering, University of Wyoming (http://weather.uwyo.edu/upperair/sounding.html), while the vertical profile of O_3 data were obtained from the Measurement of Ozone by Airbus In-Service Aircraft

ACPD
12, 29025–29067, 2012

project (MOZAIC, http://mozaic.aero.obs-mip.fr/web/). It should be noted that the vertical meteorological data presented here were obtained from the King's Park station (site 45004, 22.32° N, 114.17° E, with straight distances of 12 km and 5 km to TMS and TW, respectively), at 08:00 LT. Inspection of the figures suggested that fluctuation in relative humidity and potential temperature caused by inversion layers was found at the altitudes of 600–900 m on 23 October and 720–1000 m on 27 October. Furthermore, the modified bulk Richarson number (*Ri*) (Doran et al., 2003) was calculated, and the *Ri* values were 4.6 and 1.0 at the altitudes from 600 to 900 m on 23 October and from 720 to 1000 m on 27 October, respectively, indicating that the atmosphere was stable and no wind-shear turbulence existed at those elevations (Lin et al., 2007). These inversion layers suppressed dispersion of air pollutants and gave rise to high O_3 levels at high altitudes, consistent with previous studies (Lin et al., 2007; Ma et al., 2011). Indeed, the inversion layer was often (24 days of the selected 40 days) observed at the range of altitudes of 500 to 1000 m, which may be a factor that resulted in the high O_3 levels at the TMS site located at the elevation of 640 m.

3.2.4 Influence of atmospheric processes

Figure 4 presents the scatter plots of (a) *m*,*p*-xylene to ethylbenzene and (b) *i*-butane to propane at TMS and TW. Since *m*,*p*-xylene and *i*-butane are more reactive than ethylbenzene and propane, respectively, the ratios of *m*,*p*-xylene/ethylbenzene and *i*-butane/propane will decrease when photochemical reaction occurs during the air mass transport. These two pairs of ratios were much lower at TMS ($p < 0.05$), with the *m*,*p*-xylene/ethylbenzene ratio of 0.74 ± 0.04 pptv pptv^{-1} (1.66 ± 0.05 at TW) and the *i*-butane/propane ratio of 0.62 ± 0.06 pptv pptv^{-1} (0.78 ± 0.02 at TW). In addition, the ratio of alkyl nitrates to their parent hydrocarbons was also investigated. Since the lifetime of ethyl nitrate is shorter than ethane, and the lifetime of 2-butyl nitrate is longer than *n*-butane, the more aged air mass will have smaller ratio of ethyl nitrate/ethane vs. 2-butyl nitrate/*n*-butane (Roberts et al., 1998; Reeves et al., 2007). The ratio of ethyl nitrate/ethane vs 2-butyl nitrate/*n*-butane was 0.17 ± 0.01 at TMS, while it was

ACPD
12, 29025–29067, 2012

0.91 ± 0.10 at TW. The results suggested that the air mass arriving at TMS was generally more aged than that at TW, which may be attributed to regional transport (Guo et al., 2009; Cheng et al., 2010a) and/or mesoscale circulations, i.e., mountain-valley breezes.

Regional transport

Different wind fields were observed at TMS and TW, indicating the influence of different air masses. The combined wind roses (Fig. 5) during the sampling period clearly demonstrated that the dominated surface wind at TMS was generally from north with the dominant wind speeds between 0.02 and 4 $m\,s^{-1}$, whereas the prevailing winds were generally from southeast with dominated wind speeds of 1–3 $m\,s^{-1}$ at TW. Moreover, the diurnal wind patterns showed a clear diurnal shift in wind direction at TW, from easterly winds at night and early morning to stronger southerly winds in the afternoon (Fig. 2a, b). On the other hand, the winds at TMS were generally from the north, with increased speeds at night and in the early morning, and decreased speeds during daytime hours. The two different wind patterns indicated that O_3 mixing ratios at TMS and TW may be influenced by different air flows.

The urban centers in the PRD region of China, located with straight distances of 15–184 km north of the TMS site, are sources of air pollutants, including O_3 and its precursors (Chan and Chan, 2000; Huang et al., 2006; Guo et al., 2009). In high wind speed ($> 2\,m\,s^{-1}$), interregional transport of air pollutants generated from the PRD region could arrive in Hong Kong in several hours, thereby increasing the levels of O_3 and its precursors, as observed in many previous studies (Wang et al., 2005, 2009; Huang et al., 2006; Zhang et al., 2007; HKEPD, 2012). To investigate the effect of regional transport from the PRD region on the air pollutants at the TMS site, we examined the levels of air pollutants under the influence of regional transport, i.e. northerly winds with high speed ($> 2\,m\,s^{-1}$) and local emissions, i.e. southerly and easterly winds with low speed ($< 2\,m\,s^{-1}$). O_3, CO, SO_2 and TVOCs showed higher mixing ratios ($p < 0.05$) in the northerly winds (270° < wind direction ≤ 360° and 0° ≤ wind direction < 90°),

ACPD
12, 29025–29067, 2012

with average values of 57 ± 2 ppbv, 495 ± 9 ppbv, 4.6 ± 0.2 ppbv and 47 ± 7 ppbC, respectively, while the respective average concentrations were 48 ± 2 ppbv, 370 ± 11 ppbv, 3.6 ± 0.2 ppbv and 33 ± 7 ppbC for southerly winds (90° ≤ wind direction ≤ 270°), respectively. This feature was consistent with previous studies (Chan and Chan, 2000; Guo et al., 2009). The higher levels of air pollutants in the prevailing northerly wind compared to the weaker southerly and easterly wind further confirmed that the air pollutants at TMS were somewhat influenced by regional air masses from the highly polluted PRD region. Note that the mixing ratios of NO were comparable ($p > 0.05$, data not shown) between the prevailing northerly wind and the weaker southerly and easterly wind, which may be attributed to the fact that NO was mostly influenced by local emissions due to its short lifetime (Simpson et al., 2010).

Mesoscale circulation

To investigate the influence of mountain-valley breezes on air mass transport during this study, correlations of SO_2 and CO at the TMS and TW sites were analyzed. Figure 6a, b shows correlations of daytime and nighttime averages of CO and SO_2 for TMS versus TW. In general, moderate to good correlations were found for both CO (R^2 = 0.73 and 0.63 for daytime and nighttime hours, respectively) and SO_2 (R^2 = 0.62 and 0.69 for daytime and nighttime hours, respectively) between the two sites, suggesting some interplays of air masses. The slopes, which were less than one, imply the dilution of air masses during their transport from TW to TMS. Note that the prevailing winds at the mountain site were mainly from the north while those at TW were mostly from southeast (Fig. 2a). It is unlikely that the correlations for TMS versus TW were caused by the same regional air mass. Therefore, it suggested that the interplays of air masses and the moderate to good correlations between the two sites were likely caused by the influence of mesoscale circulations, i.e. mountain-valley breezes. The lower correlation for CO observed during the nighttime hours was likely due to the fact that the observed CO concentrations at TW were higher because of the local urban emissions. The lower correlation for SO_2 during daytime hours was driven by a few

ACPD
12, 29025–29067, 2012

data points with higher observed than predicted SO_2 levels at TMS. This is mostly attributed to the influence of regional transport (Sect. 3.2.4) which could bring the air pollutants from the PRD region to TMS (Fig. 6b).

The correlation between the observation and the results of moving box (Mbox) model for TMS and TW developed by the PBM-MCM was also explored to evaluate the influence of mesoscale circulation. It should be noted that the scenario in the Mbox model is an over simplified mountain-valley breezes phenomenon with the grid sits between TW and TMS monitoring stations and an air parcel moving on an idealized trajectory. After simulation, the Mbox calculated O_3 was compared to the observed O_3 at TMS and TW during daytime (08:00–17:00 LT) and nighttime (18:00–07:00 LT), respectively (Fig. 7). The time lag between the two sites was evaluated from dividing the distance between TMS and TW by the average value of the observed wind speed during daytime and nighttime hours. The value of time lag was factored in for pairs of data points used for correlation analysis, i.e. a sample collected at 09:00 LT at TW corresponded to a sample at 10:00 LT at TMS for a valley breeze during daytime hours if the time difference is 1 h, and vice versa during nighttime hours when there is mountain breezes. Good correlation (R^2 = 0.70) between Mbox model O_3 vs. observed O_3 was found during daytime (Fig. 7a), while no association (R^2 = 0.02) was found in nighttime hours (Fig. 7b). During nighttime, TMS was assumed to be the center of the box model and the concentrations of air pollutants at this site, i.e. VOCs and trace gases, were used for the model simulation. The model did not take into account the NO (which could titrate O_3 as previously discussed) emitted locally at TW and/or the dry deposition of O_3 (Cheng et al., 2010b; Lam et al., 2012), resulting in the higher levels of simulated O_3 at TW. On the other hand, the good correlation during daytime suggested that O_3 at TMS was related to the air pollutants at TW, indicating the influence of mesoscale circulations.

In addition to the above analysis, mountain-valley breezes were simulated using a domain system of five nested grids (Sect. 2.3). The modeling focused on 16–18, 23 September, 23–24, 29–31 October, 1–3, 9, 12, and 19 November 2010, when evidence

ACPD
12, 29025–29067, 2012

for the mesoscale circulation was clear based on the meteorological data and the levels of air pollutants. Here, the simulation results for 9 November are presented as an example (Fig. 8).

The outer four nested domains were simulated using a two-way interactive method from 00:00 UTC (08:00 LT) on 8 November, which was initialized using NCEP FNL $1^\circ \times 1^\circ$ reanalysis data, while the inner domain was simulated using a one-way nested method from 12:00 UTC (20:00 LT) on 8 November, with initial and boundary fields provided by the fourth domain (1.333 km grid). The model results showed that, although the dominant synoptic wind direction was from the north during daytime and nighttime hours, weak mesoscale flows was observed. The model simulation showed a valley breeze in daytime (09:00 LT) on 9 November and a mountain breeze during nighttime (23:00 LT) hours. Therefore, the model simulation results further confirmed the influence of mountain-valley breezes on the redistribution of air pollutants between TW and TMS. Since O_3 is a secondary pollution, as the air masses aged, secondary reactions occurred and the accumulated O_3 pollution increased (Jiang et al., 2010). Mesoscale circulations, i.e. mountain-valley breeze, can bring freshly-emitted precursors such as VOCs and newly-formed O_3 including that formed during the transit from the urban areas at the foot of the mountain (i.e. TW) to the summit (i.e. TMS) during daytime hours, which induced higher O_3 levels at TMS.

In summary, based on the above discussion, it could be concluded that the higher O_3 mixing ratios at TMS was attributed to the combination influence of NO titration, vertical meteorological conditions, and different atmospheric processes including mesoscale circulations and regional transport.

3.3 The relationships between O_3 and its precursors

Correlations between O_3 and reactive nitrogen (NO_y) can provide useful information on the chemistry of photochemical O_3 formation in a given location (Sillman et al., 1998 and references therein). In this study, NO was detected with a chemiluminescence analyzer (API, Model 200E), while NO_2 was converted to NO by a hot molybdenum oxide

ACPD
12, 29025–29067, 2012

(MoO) convertor and measured by the chemiluminescene detector. This analysis technique converts not only NO_2 but also other reactive nitrogen species, including peroxyacetyl nitrate anhydride (PAN), organic nitrates and nitric acid to NO (Wang et al., 2001; Steinbacher et al., 2007; Xu et al., 2012). The "NO_x" measured, defining as "NO_x^*", is thus the sum of NO, NO_2 and other reactive nitrogen species described above, which approximate to NO_y levels in the atmosphere (Wang et al., 2001; Steinbacher et al., 2007; Xu et al., 2012). As such, the measured NO_x^* was taken as a surrogate of NO_y in this study.

Since the range of peak O_3 levels was large at TMS, correlations between O_3 and NO_x^* were investigated for six scenarios, which were divided according to different ranges of the peak one-hour average O_3 mixing ratio. Figure 9 presents the correlations of O_3 with NO_x^* for the 10-min average data during the photochemical active hours (10:00–18:00, LT) in different O_3 scenarios. Negative correlations between O_3 and NO_x^* were found at TMS in the scenarios with lower O_3 levels (the highest hourly average of 20–80 ppbv). This feature suggested a VOC-sensitive regime, where the photochemical O_3 formation was suppressed as NO_x mixing ratios increased (with average NO_x^* levels changing from 7.8 ± 0.4 to 13.4 ± 0.8 ppbv) in the corresponding scenarios. However, correlations deteriorated when O_3 levels were higher (the highest hourly average of 80–140 ppbv), indicating that the suppression of NO_x^* reduced and photochemical O_3 formation had changed from VOC-sensitive to both VOC- and NO_x-sensitive as O_3 levels increased (Sillman et al., 2003).

Figure 10 shows the scatter plots of O_3 and NO_x^* during the photochemical active hours (10:00–18:00 LST) at TW. The results indicated that O_3 concentrations were negatively correlated with NO_x^*, implying that O_3 formation was primarily VOC-sensitive at TW (Sillman et al., 2003).

The ratio of VOC_s/NO_x (NO + NO_2) is an important parameter to evaluate the relationships between O_3 and its precursors (Sillman, 1999; Jenkin et al., 2000). Previous studies (Dodge, 1977; Finlayson-Pitts and Pitts, 1993; NESCAUM, 1995; Jenkin et al., 2000) found that the VOC_s/NO_x ($\mathrm{ppmC\,ppm^{-1}}$) ratio of 8 is an approximate

ACPD
12, 29025–29067, 2012

reference point for evaluating relative benefits of NO_x and VOC controls. O_3 could be effectively reduced by a decrease of VOC under VOC-limited conditions, with the ratio of $VOC/NO_x < 4/1$; and by a reduction of NO_x concentration under NO_x-limited conditions, with the ratio of $VOC/NO_x > 15/1$. In the transition area, when the ratios range from 4/1 to 15/1, a combination of VOC and NO_x controls is needed. Figure 11 shows the range of measured VOCs versus NO_x during daytime hours at TW and TMS. At TW, about 82 % of data points had VOC/NO_x ratio within the range of 1 to 4, while the ratio for 17 % of data points was ranging from 4 to 8. This result indicated that photochemical O_3 formation was mainly VOC-limited at TW; therefore, VOC reduction was most effective in reducing O_3, and increasing NO_x would suppress O_3 formation. On the other hand, different characteristics were observed at TMS. Most of the data points (about 60 %) had the ratios in the transition area, with values of 4 to 15, while the rest 40 % of data points had values ranging from 1 to 4. Additionally, about 96 % of those data points with ratios ranging from 4 to 15, were found to range from 4 to 8. The relatively higher ratios of VOC/NO_x at TMS indicated that though VOCs were the most important compounds in the production of O_3 at TMS, while the contribution of NO_x was also significant and a combination of VOC and NO_x reductions may be warranted.

To help further understand the relative importance of VOCs on photochemical O_3 formation at the two sites, a propylene-equivalent concentration method (Chameides et al., 1992), was adopted for different groups of VOCs in this study. The propylene-equivalent concentration for VOC species can be calculated as Eq. (6),

$$\text{Propy-Equiv}(J) = C_J \times k_{OH}(J)/k_{OH}(C_3H_6) \quad (6)$$

where Propy-Equiv (J) is a measure of the concentration of VOC species J on an OH-reactivity-based sacle normalized to the reactivity of propylene, k_{OH} (J) is the rate constant between species J and OH radical (Atkinson, 2000), and k_{OH} (C_3H_6) is the rate constant between C_3H_6 and OH radical. Figure 12 shows the apportionment of pro-equiv for different VOC groups at TMS and TW in daytime hours (07:00–18:00 LT) during the sampling period. It was found that the contributions of the groups of R-OLE

ACPD
12, 29025–29067, 2012

and $C \geq 4$ were lower ($p < 0.05$) at TMS than TW, while the contributions of LRHC, ETH and R-AROM were comparable at the two sites. In particular, much higher contributions of BVOCs were found at TMS than TW. Further inspection of the figure revealed that aromatic species, i.e. xylenes, toluene, ethylbenzene and trimethylbenzenes, and biogenic VOC species, including isoprene, α/β-pinene and limonene were the two important VOC groups (about 70 %) that contributed most to the photochemical O_3 formation at TMS and TW. This feature suggested that O_3 formation at TMS and TW can be mainly attributed to a small number of VOC species, consistent with previous studies (Zhang et al., 2007; Cheng et al., 2010a), which could provide a scientific basis for the development of effective regulations to the control of photochemical smog in Hong Kong.

4 Conclusions

Simultaneous systematic measurements of air pollutants were conducted at the foot and near the summit of a mountain in Hong Kong from September to November 2010. The levels of primary air pollutants (i.e. CO, SO_2, NO_x and VOCs) were lower at TMS than TW, while O_3 was greater at TMS than TW. Only 1 O_3 episode day and 3 near O_3 episode days were observed at TW, while a total 21 O_3 episode days were found at TMS. The relatively higher levels of O_3 at TMS were attributed to the combination effects of NO titration, vertical meteorological conditions, regional transport and mesoscale circulations. On the other hand, the correlations over the entire ranges of observed O_3 and NO_x^* implied that photochemical O_3 formation is VOC-sensitive or both NO_x and VOC-sensitive at TMS, while it was VOC-sensitive at TW. The relatively higher ratios of VOC/NO_x at TMS indicated that although VOCs were the most important compounds in the O_3 production at TMS, the contribution of NO_x was also significant. The results of propylene-equivalent concentration for VOC species further suggested that photochemical O_3 formation at TMS ad TW was attributed to a small number of VOC species.

ACPD
12, 29025–29067, 2012

Acknowledgement. This project is supported by the Research Grants Council of the Hong Kong Special Administrative Region via grants PolyU5179/09E and N_PolyU545/09. This study is partly supported by the internal grants of the Hong Kong Polytechnic University (A-PK25 and 1-ZV7A). The authors acknowledge for the strong support of the European Commission, Airbus, and the Airlines (Lufthansa, Austrian, Air France) who carry free of charge the MOZAIC equipment and perform the maintenance since 1994. MOZAIC is presently funded by INSU-CNRS (Institute National des Sciences del'Univers – Centre National de la Recherche Scientifique, France), Météo-France, and FZJ (Forschungszentrum Jülich, Germany). The Final Analysis Data (FNL) was obtained from NOAA CDC.

References

AFCD (Agriculture, Fisheries and conservation Department): available at: http://www.afcd.gov.hk/, 2008.

Atkinson, R.: Gas-phase tropospheric chemistry of volatile organic compounds: 1. Alkanes and alkenes, J. Phys. Chem. Ref. Data, 26, 215–291, 1997.

Atkinson, R.: Atmospheric chemistry of VOCs and NO_x, Atmos. Environ., 34, 2063–3101, 2000.

Bloss, C., Wagner, V., Jenkin, M. E., Volkamer, R., Bloss, W. J., Lee, J. D., Heard, D. E., Wirtz, K., Martin-Reviejo, M., Rea, G., Wenger, J. C., and Pilling, M. J.: Development of a detailed chemical mechanism (MCMv3.1) for the atmospheric oxidation of aromatic hydrocarbons, Atmos. Chem. Phys., 5, 641–664, doi:10.5194/acp-5-641-2005, 2005.

Burley, J. D. and Bytnerowicz, A.: Surface ozone in the white mountains of California, Atmos. Environ., 45, 4591–4602, 2011.

Chameides, W. L., Fehsenfeld, F., Fodgers, M. O., Cardelino, C., Martinez, J., Parrish, D., Lonneman, W., Lawson, D. R., Rasmussen, R. A., Zimmerman, P., Greenberg, J., Mlddleton, P., and Wang, T.: Ozone precursor relationships in the ambient atmospheric, J. Geophys. Res., 97, 6037–6055, 1992.

Chan, C. Y. and Chan, L. Y.: Effect of meteorology and air pollutant transport on ozone episodes at a subtropical coastal Asian city, Hong Kong, J. Geophys. Res., 105, 20707–20724, 2000.

Chan, L. Y., Chan, C. Y., and Qin, Y.: Surface ozone pattern in Hong Kong, J. Appl. Meteorol., 37, 1153–1165, 1998a.

Chan, L. Y., Liu, H. Y., and Lam, K. S.: Analysis of the seasonal behavior of tropospheric ozone at Hong Kong, Atmos. Environ., 32, 159–168, 1998b.

Chen, C. L., Tsuang, B. J., Tu, C. Y., Cheng, W. L., and Lin, W. D.: Wintertime vertical profiles of air pollutants over a suburban area in central Taiwan, Atmos. Environ., 36, 2049–2059, 2002.

Cheng, H. R., Guo, H., Wang, X. M., Saunders, S. M., Lam, S. H. M., Jiang, F., Wang, T., Ding, A., Lee, S., and Ho, K. F.: On the relationship between ozone and its precursors in the Pearl River Delta: application of an observation-based model (OBM), Environ. Sci. Pollut. Res., 17, 547–560, 2010a.

Cheng, H. R., Guo, H., Saunders, S. M., Lam, S. H. M., Jiang, F., Wang, X. M., Simpson, I. J., Blake, D. R., Louie, P. K. K., and Wang, T. J.: Assessing photochemical ozone formation in the Pearl River Delta with a photochemical trajectory model, Atmos. Environ., 44, 34, 4199–4208, 2010b.

Colman, J. J., Swanson, A., Meinardi, S., Sive, B. C., Blake, D. R., and Rowland, F. S.: Description of the analysis of a wide range of volatile organic compounds in whole air samples collected during PEM-Tropics A and B, J. Anal. Chem., 73, 3723–3731, 2001.

Crowley, J. N., Schuster, G., Pouvesle, N., Parchatka, U., Fischer, H., Bonn, B., Bingemer, H., and Lelieveld, J.: Nocturnal nitrogen oxides at a rural mountain-site in south-western Germany, Atmos. Chem. Phys., 10, 2795–2812, doi:10.5194/acp-10-2795-2010, 2010.

Ding, A. J., Wang, T., Zhao M., Wang, T. J., and Li, Z. K.: Simulation of sea-land breezes and a discussion of their implications on the transport of air pollution during a multi-day ozone episode in the Pearl River Delta of China, Atmos. Environ., 38, 6737–6750, 2004.

Dodge, M. C.: Combined use of modeling techniques and smog chamber data to derive ozone-precursor relationships. International Conference on Photochemical Oxidant Pollution and its Control: Proceedings, Vol.II B, EPA/600/3-77-001b, US Environmental Protection Agency, Research Triange Park, NC, 881–889, 1977.

Done, J., Davis, C., and Weisman, M.: The next generation of NWP: explicit forecasts of convection using the Weather Research and Forecast (WRF) model, Atmos. Sci. Lett., 5, 110–117, doi:10.1002/asl.72, 2004.

Doran, J. C., Berkowitz, C. M., Coulter, R. L., Spicer, C. W., and Shaw, W. J.: The 2001 Phoenix Sunrise experiment: vertical mixing and chemistry during the morning transition in Phoenix, Atmos. Environ., 37, 2365–2377, 2003.

ACPD
12, 29025–29067, 2012

Evtyugina, M. G., Nunes, T., Alves, C., and Marques, M. C.: Photochemical pollution in a rural mountainous area in the northeast of Portugal. Atmos. Res., 92, 151–158, 2009.
Finlayson-Pitts, B. J. and Pitts, N.: VOCs, NO_x and ozone production, J. Air Waste Manage. Assoc., 43, 1093–1101, 1993.
Fu, P. Q., Kawamura, K., Kanaya, Y., and Wang, Z. F.: Contributions of biogenic volatile organic compounds to the formation of secondary organic aerosols over Mt. Tai, Central East China, Atmos. Environ., 44, 4817–4826, 2010.
Gao, J., Wang, T., Ding, A. J., and Liu, C. B.: Observational study of ozone and carbon monoxide at the summit of mount Tai (1534 m a.s.l.) in Central-Eastern China, Atmos. Environ., 39, 4779–4791, 2005.
Guo, H., Jiang, F., Cheng, H. R., Simpson, I. J., Wang, X. M., Ding, A. J., Wang, T. J., Saunders, S. M., Wang, T., Lam, S. H. M., Blake, D. R., Zhang, Y. L., and Xie, M.: Concurrent observations of air pollutants at two sites in the Pearl River Delta and the implication of regional transport, Atmos. Chem. Phys., 9, 7343–7360, doi:10.5194/acp-9-7343-2009, 2009.
Guo, H., Ling, Z. H., Simpson, I. J., Blake, D. R., and Wang, D. W.: Observation of isoprene, methacrolein (MAC) and methyl vinyl ketone (MVK) at a mountain site in Hong Kong, J. Geophys. Res., 117, D19303, doi:10.1029/2012JD017750, 2012.
Hong Kong Environmental Protection Department (HKEPD): Air Quality in Hong Kong 2011 (Preliminary Report), Air Science Group, Environmental Protection Department, the Government of the Hong Kong Special Administrative Region, Hong Kong, 2012.
Huang, J. P., Fung, J. C. H., and Lau, A. K. H.: Integrated processes analysis and systematic meteorological classification of ozone episodes in Hong Kong, J. Geophys. Res., 111, D20309, doi:10.1029/2005JD007012, 2006.
IPCC (Intergovernmental Panel on Climate Change): The Physical Science Basis. Contribution of Working Group I to the Fourth Assessment Report of the Intergovernmental Panel on Climate Change, Cambridge Univ. Press, Cambridge, UK, 2007.
Jenkin, M. E. and Clemitshaw, K. C.: Ozone and other secondary photochemical pollutants: chemical processes governing their formation in the planetary boundary layer, Atmos. Environ., 34, 2499–2527, 2000.
Jenkin, M. E., Saunders, S. M., Wagner, V., and Pilling, M. J.: The tropospheric degradation of volatile organic compounds: a protocol for mechanism development, Atmos. Environ., 31, 81–107, 1997.

ACPD
12, 29025–29067, 2012

Jenkin, M. E., Saunders, S. M., Wagner, V., and Pilling, M. J.: Protocol for the development of the Master Chemical Mechanism, MCM v3 (Part B): tropospheric degradation of aromatic volatile organic compounds, Atmos. Chem. Phys., 3, 181–193, doi:10.5194/acp-3-181-2003, 2003.

Jiang, F., Wang, T. J., Wang, T. T., Xie, M., and Zhao, H.: Numerical modeling of a continuous photochemical pollution episode in Hong Kong using WRF-chem, Atmos. Environ., 42, 8717–8727, 2008.

Jiang, F., Guo, H., Wang, T. J., Cheng, H. R., Wang, X. M., Simpson, I. J., Ding, A. J., Saunders, S. M., Lam, S. H. M., and Blake, D. R.: An ozone episode in the Pearl River Delta: field observation and model simulation, J. Geophys. Res., 115, D22305, doi:10.1029/2009JD013583, 2010.

Jobson, B. T., Mckeen, S. A., and Parrish, D. D.: Spatial and temporal variability of nonmethane hydrocarbon mixing ratios and their relation to photochemical lifetime, J. Geophys. Res., 103, 13557–13567, 1998.

Lam, S. H. M., Ling, Z. H., Guo, H., Saunders, S. M., Jiang, F., Wang, X. M., and Wang, T. J.: Modelling VOC source impacts on high ozone episode days observed at a mountain summit in Hong Kong under the influence of mountain-valley breezes, in preparation, 2012.

Li, J., Pochanart, P., Wang, Z. F., Liu, Y., Yamaji, K., Takigawa, M., Kanaya, Y., and Akimoto, H.: Impact of chemical production and transport on summertime diurnal ozone behavior at a mountainous site in North China Plain, Sola, 4, 121–124, 2008.

Lin, C. H., Lai, C. H., Wu, Y. L., Lai, H. C., and Lin, P. H.: Vertical ozone distributions observed using tethered ozonesondes in a coastal industrial city, Kaohsiung, in Southern Taiwan, Environ. Monit. Assess., 127, 253–270, 2007.

Lin, W., Xu, X., Zhang, X., and Tang, J.: Contributions of pollutants from North China Plain to surface ozone at the Shangdianzi GAW Station, Atmos. Chem. Phys., 8, 5889–5898, doi:10.5194/acp-8-5889-2008, 2008.

Liu, Y., Shao, M., Kuster, W. C., Goldan, P. D., Li, X. H., Lu, S. H., and de Gouw, J. A.: Source identification of reactive hydrocarbons and oxygenated VOCs in the summertime in Beijing, Environ. Sci. Technol., 43, 75–81, 2009.

Ma, Z. Q., Zhang, X. L., Xu, J., Zhao, X. J., and Wei, M.: Characteristics of ozone vertical profile observed in the boundary layer around Beijing in autumn, J. Environ. Sci., 23, 1316–1324, 2011.

ACPD
12, 29025–29067, 2012

Monteiro, A., Strunk, A., Carvalho, A., Tchepep, O., Miranda, A. I., Borrego, C., Saavedra, S., Rpdríguez, A., Souto, J., Casares, J., Friese, E., and Elbern, H.: Investigating a high ozone episode in a rural mountain site, Environ. Pollut,, 162, 176–189, 2012.

NESCAUM (Northeast States for Coordinated Air Use Management), 1995: Preview of 1994.

NRC (National Research Council): The effects of meteorological on tropospheric ozone, in: Rethinking the ozone problem in urban and regional air pollution, National Academy Press, Washington, DC, USA, 1991.

Ou Yang, C. F., Liu, N. H., Sheu, G. R., Lee, C. T., and Wang, J. L.: Seasonal and diurnal variations of ozone at a high-altitude mountain baseline station in East Asia, Atmos. Environ., 46, 279–288, 2012.

Parrish, D. D., Buhr, M. P., Trainer, M., Northon, R. B., Shimshock, J. P., Fehsenfeld, F. C., Anlauf, K. G., Bottenheim, J. W., Tang, Y. Z., Wiebe, H. A., Roberts, J. M., Tanner, R. L., Newman, L., Bowersox, V. C., Olszyna, K. J., Bailey, E. M., Rodgers, M. O., Wang, T., Berresheim, H., Roychowdhury, U. K., and Demerjiani, K. L.: The total reactive oxidized nitrogen levels and their partitioning between the individual species at six rural sites in Eastern North America, J. Geophys. Res., 98, 2927–2939, 1993.

PORG (Photochemical Oxidants Review Group): Ozone in the United Kingdom, Fourth Report of the UK photochemical Oxidants review group, Department of the Environment, Transport and the Regions, London, 1997.

Pochanart, P., Akimoto, H., Kajii, Y., Potemkin, V. M., and Khodzher, V. T.: Regional background ozone and carbon monoxide variations in remote Siberia/East Asia, J. Geophys. Res., 108, 4028, 2003.

Reeves, C. E., Slemr, J., Oram, D. E., Worton, D., Penkett, S. A., Stewart, D. J., Purvis, R., Watson, N., Hopkins, J., Lewis, A., Methven, J., Blake, D. R., and Atlas, E.: Alkyl nitrates in outflow from North America over the North Atlantic during Intercontinental Transport of Ozone and Precursors 2004, J. Geophys. Res., 112, D10S37, doi:10.1029/2006JD007567, 2007.

Roberts, J. M., Bertman, S. B., Parrish, D. D., Fehsenfeld, F. C., Jobson, B. T., and Niki, H.: Measurement of alkyl nitrates at Chebogue Point, Nova Scotia during the 1993 North Atlantic Regional Experiment (NARE) intensive, J. Geophys. Res., 103, 13569–13580, 1998.

Scott, B. and Ahmet, P.: Influence of synoptic and mesoscale meteorology on ozone pollution potential for San Joaquin Valley of California, Atmos. Environ., 43, 1779–1788, 2009.

ACPD
12, 29025–29067, 2012

Sillman, S.: The relation between ozone, NO_x and hydrocarbons in urban and polluted rural environments, Atmos. Environ., 33, 1821–1845, 1999.

Sillman, S., He, D. Y., and Pippin, M. R.: Model correlations for ozone, reactive nitrogen, and peroxides for Nashville in comparison with measurements: Implications for O_3-NO_x-hydrocarbon chemistry, J. Geophys. Res., 103, 22629–22644, 1998.

Sillman, S., Vautard, R., Menut, L., Kley, D.: O_3-NO_x-VOC sensitivity and NO_x-VOC indicators in Paris: results from models and atmospheric pollution over the Paris Area (ESQUIF) measurements, J. Geophys. Res., 108, 8563, doi:10.1029/2002JD001561, 2003.

Simpson, I. J., Blake, N. J., Barletta, B., Diskin, G. S., Fuelberg, H. E., Gorham, K., Huey, L. G., Meinardi, S., Rowland, F. S., Vay, S. A., Weinheimer, A. J., Yang, M., and Blake, D. R.: Characterization of trace gases measured over Alberta oil sands mining operations: 76 speciated C_2–C_{10} volatile organic compounds (VOCs), CO_2, CH_4, CO, NO, NO_2, NO_y, O_3 and SO_2, Atmos. Chem. Phys., 10, 11931–11954, doi:10.5194/acp-10-11931-2010, 2010.

Skamarock, W. C. and Klemp, J. B.: A time split non hydrostatic atmospheric model for weather research and forecasting applications, J. Comput. Phys., 227, 7, 3465–3485, 2008.

So, K. L. and Wang, T.: On the local and regional influence on ground-level ozone concentrations in Hong Kong, Environ. Pollut., 123, 307–317, 2003.

Steinbacher, M., Zellweger, C., Schwarzenbach, B., Bugmann, S., Buchmann, B., Ordónez, C., Prevot, A., and Hueglin, C.: Nitrogen oxide measurements at rural sites in Switzerland: Bias of conventional measurement techniques, J. Geophys. Res., 112, D11307, 2007.

Steven E. K., Benjamin, S. G., McGinley, J. A., Brown, J. M., Schultz, P., Szoke, E. J., Smirnova, T. G., Shaw, B. L., Birkenheuer, D., Albers, S., Peckham, S., Grell, G.: Real-time Applications of the WRF Model at the Forecast Systems Laboratory, 84th AMS Annual Meeting, Seattle, USA, 10–15 January 2004.

Tang, G., Wang, Y., Li, X., Ji, D., Hsu, S., and Gao, X.: Spatial-temporal variations in surface ozone in Northern China as observed during 2009–2010 and possible implications for future air quality control strategies, Atmos. Chem. Phys., 12, 2757–2776, doi:10.5194/acp-12-2757-2012, 2012.

Tseng, K. H., Chen, C. L., Lin, M. D., Chang, K. H., and Tsuang, B. J.: Vertical profile of ozone and accompanying air pollutant concentrations observed at a downwind foothill site of industrial and urban areas, Aerosol Air Qual. Res., 9, 421–434, 2009.

ACPD
12, 29025–29067, 2012

Turnipseed, A. A., Anderson, D. E., Burns, S., Blanken, P. D., and Monson, R. K.: Airflows and turbulent flux measurements in mountainous terrain Part 2: mesoscale effects, AGR. Forest Meterol., 125, 187–205, 2004.

Wang, T., Cheung, V. T. F., Lam, K. S., Kok, G. L., and Harris, J. M.: The characteristics of ozone and related compounds in the boundary layer of the South China coast: temporal and vertical variations during autumn season, Atmos. Environ., 35, 2735–2746, 2001.

Wang, T., Poon, C. N., Kwok, Y. H., and Li, Y. S.: Characterizing the temporal variability and emission patterns of pollution plumes in the Pearl River Delta of China, Atmos. Environ., 37, 3539–3550, 2003.

Wang, T., Guo, H., Blake, D. R., Kwok, Y. H., Simpson, I. J., and Li, Y. S.: Measurements of trace gases in the inflow of South China Sea background air and outflow of regional pollution at Tai O, Southern China, J. Atmos. Chem., 52, 295–317, 2005.

Wang, T., Wong, H. L. A., Tang, J., Ding, A., Wu, W. S., and Zhang, X. C.: On the origin of surface ozone and reactive nitrogen observed at remote site in the northeastern Qinghai-Tibetan Plateau, Western China, J. Geophys. Res., 111, D08303, doi:10.1029/2005JD006527, 2006.

Wang, T., Wei, X. L., Ding, A. J., Poon, C. N., Lam, K. S., Li, Y. S., Chan, L. Y., and Anson, M.: Increasing surface ozone concentrations in the background atmosphere of Southern China, 1994–2007, Atmos. Chem. Phys., 9, 6217–6227, doi:10.5194/acp-9-6217-2009, 2009.

Xu, Z., Wang, T., Xue, L. K., Louie, P., Luk, C., Gao, J., Wang, S. L., Chai, F. H., and Wang, W. X.: Evaluating the uncertainties of thermal catalytic conversion for measuring atmospheric nitrogen dioxide at four polluted sites in China, Atmos. Environ., doi:10.1016/j.atmosenv.2012.09.043, in press, 2012.

Xue, L. K., Wang, T., Zhang, J. M., Zhang, X. C., Delig-Geer, Poon, C. N., Ding, A. J., Zhou, X. H., Wu, W. S., Tang, J., Zhang, Q. Z., and Wang, W. X.: Source of surface ozone and reactive nitrogen speciation at Mount Waliguan in Western China: new insights from the 2006 summer study, J. Geophys. Res., 116, D07306, doi:10.1029/2010JD014735, 2011.

Zellweger, C., Forrer, J., Hofer, P., Nyeki, S., Schwarzenbach, B., Weingartner, E., Ammann, M., and Baltensperger, U.: Partitioning of reactive nitrogen (NO_y) and dependence on meteorological conditions in the lower free troposphere, Atmos. Chem. Phys., 3, 779–796, doi:10.5194/acp-3-779-2003, 2003.

ACPD
12, 29025–29067, 2012

Zhang, J., Wang, T., Chameides, W. L., Cardelino, C., Kwok, J., Blake, D. R., Ding, A., and So, K. L.: Ozone production and hydrocarbon reactivity in Hong Kong, Southern China, Atmos. Chem. Phys., 7, 557–573, doi:10.5194/acp-7-557-2007, 2007.

ACPD
12, 29025–29067, 2012

Table 1. Statistics of trace gases at the TMS and TW sites.

Species	TMS		TW	
	Mean ± 95 % CI*	Max value	Mean ± 95 % CI*	Max value
O_3 (ppbv)	55 ± 1	163	22 ± 1	116
O_x (ppbv)[1]	58 ± 1	178	47 ± 1	157
NO_x (ppbv)[2]	10.7 ± 0.3	75	55 ± 1	262
CO (ppbv)	436 ± 7	842	517 ± 8	1150
SO_2 (ppbv)	4.1 ± 0.1	28	6.1 ± 0.2	31

* Mean ±95 % confidence intervals.
[1] $O_x = NO_2 + O_3$.
[2] $NO_x = NO + NO_2$.

ACPD
12, 29025–29067, 2012

Fig. 1. The sampling sites and the surrounding environment.

ACPD
12, 29025–29067, 2012

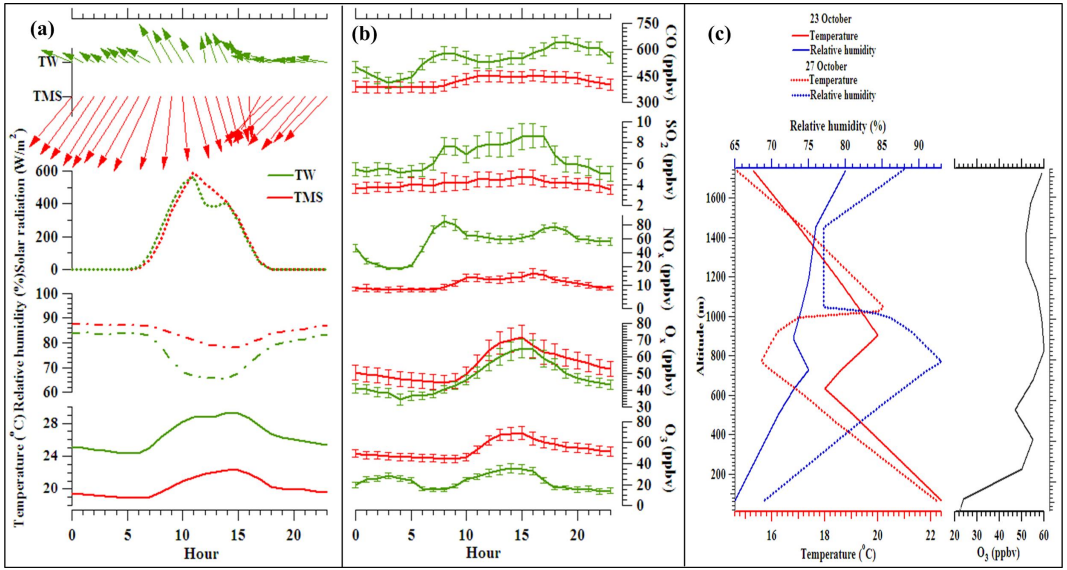

Fig. 2. (a) Surface meteorological conditions and **(b)** trace gases average diurnal patterns at TMS and TW and **(c)** vertical profiles of meteorological condition and O_3 in Hong Kong.

ACPD
12, 29025–29067, 2012

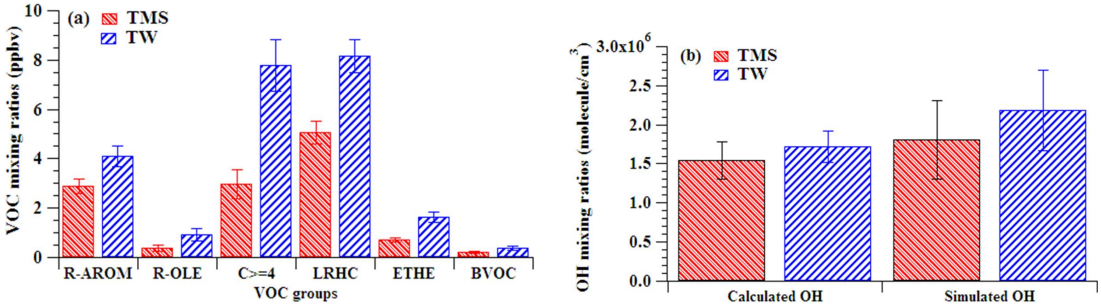

Fig. 3. The mean mixing ratios of **(a)** different VOC species and **(b)** OH radical at TMS and TW during the sampling period. Vertical bars are 95 % confidence intervals.

ACPD
12, 29025–29067, 2012

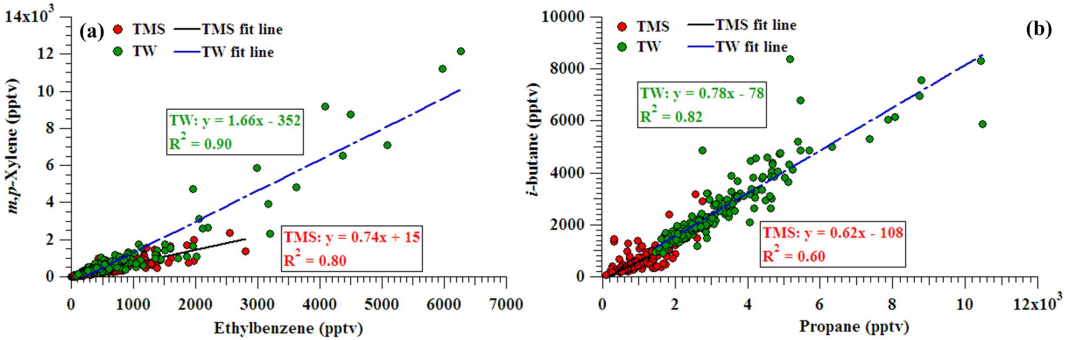

Fig. 4. The scatter plots of **(a)** *m*,*p*-xylene vs. ethylbenzene and **(b)** *i*-butane vs. propane at TMS and TW.

ACPD
12, 29025–29067, 2012

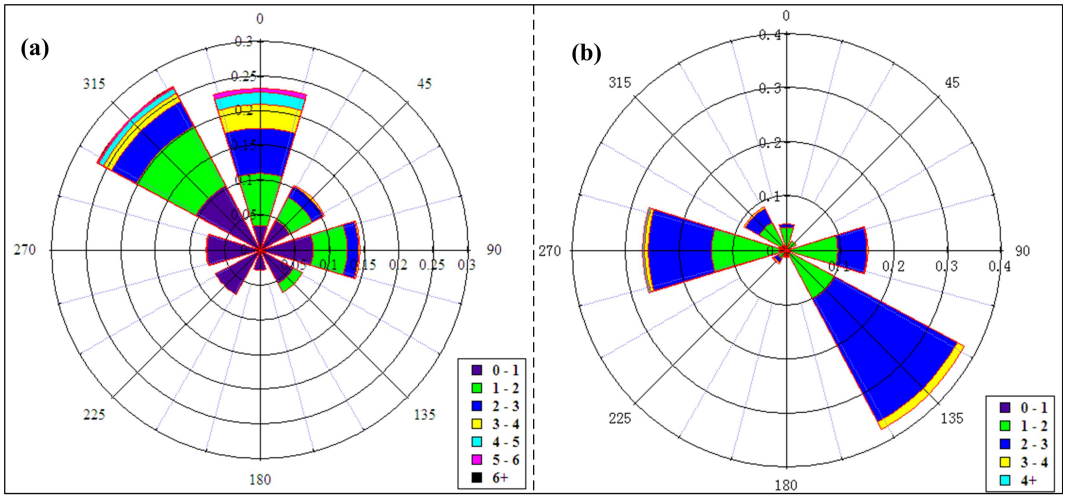

Fig. 5. Combined wind rose maps at daytime hours during the sampling period at **(a)** TMS and **(b)** TW.

ACPD
12, 29025–29067, 2012

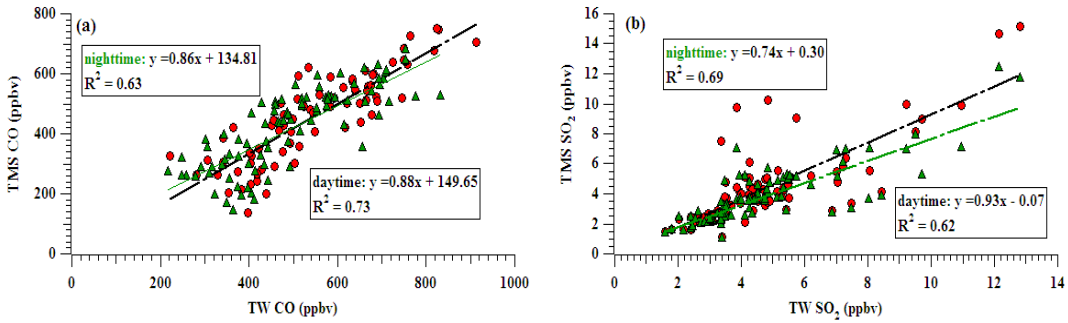

Fig. 6. Scatter plots of **(a)** CO and **(b)** SO_2 during daytime and nighttime hours between TMS and TW.

ACPD
12, 29025–29067, 2012

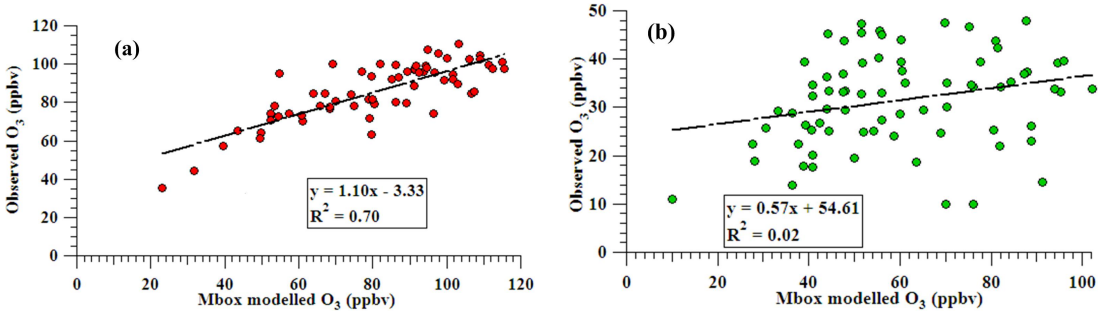

Fig. 7. The correlation between the observed data and the MCM modeled results during **(a)** daytime and **(b)** nighttime hours.

ACPD
12, 29025–29067, 2012

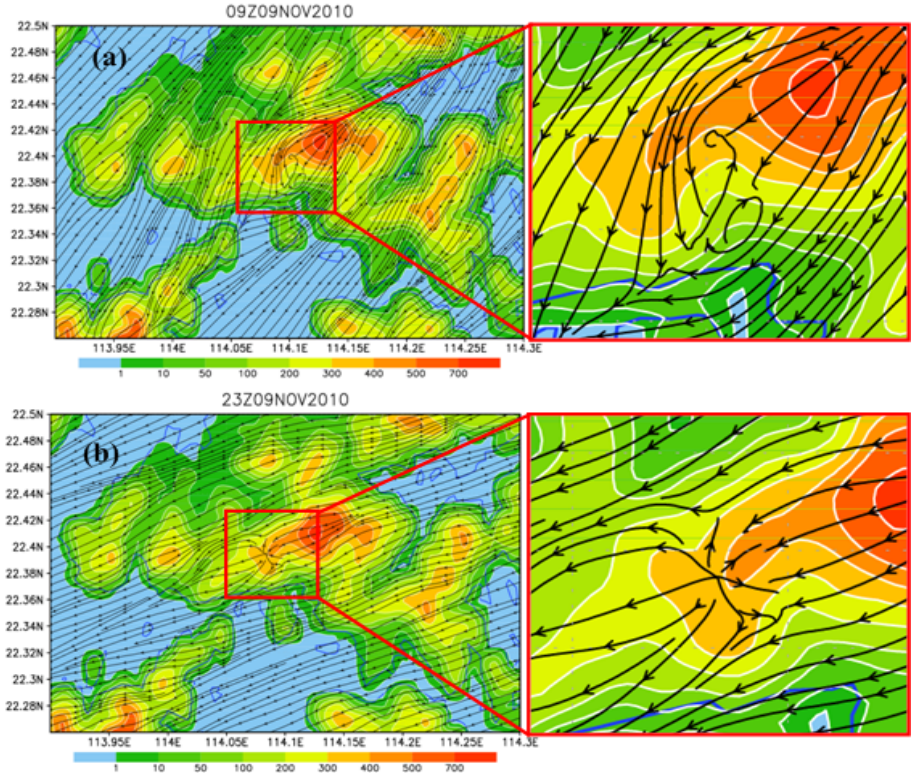

Fig. 8. Simulation of mountain-valley breezes on 9 November 2010: **(a)** valley breezes at daytime; **(b)** mountain breezes at nighttime.

ACPD
12, 29025–29067, 2012

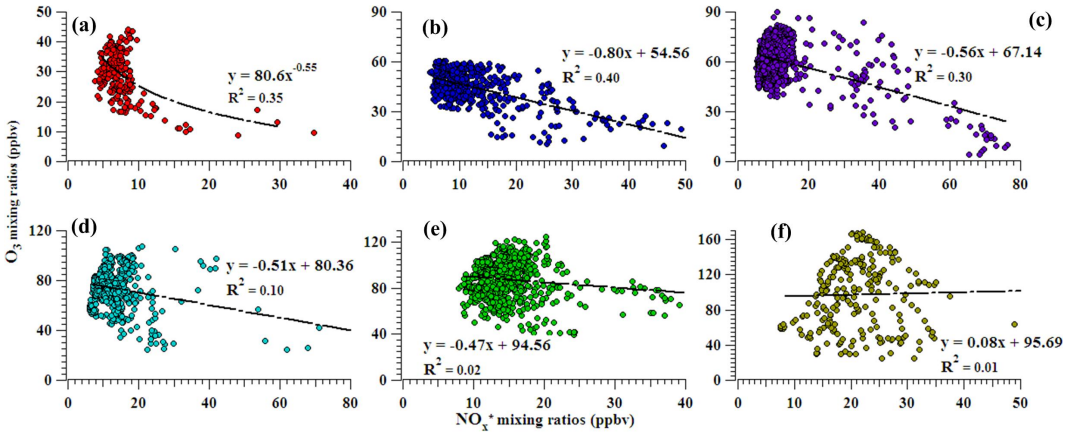

Fig. 9. Scatter plots of O_3 (ppbv) versus NO_x^* (ppbv) for the days with the hourly peak O_3 of **(a)** $20 \leq O_3 \leq 40$; **(b)** $40 < O_3 \leq 60$; **(c)** $60 < O_3 \leq 80$; **(d)** $80 < O_3 \leq 100$; **(e)** $100 < O_3 \leq 120$; **(f)** $O_3 > 120$ at TMS during sampling period.

ACPD
12, 29025–29067, 2012

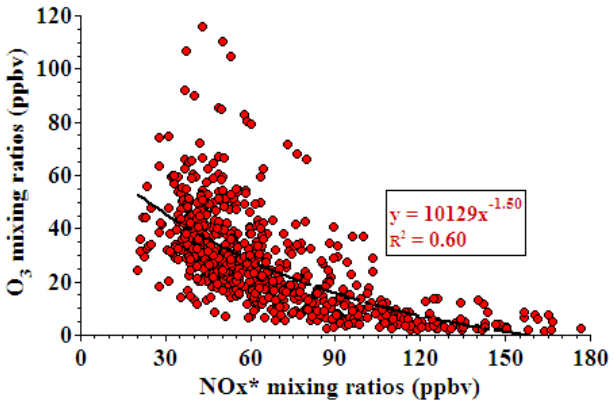

Fig. 10. Scatter plot of O_3 (ppbv) versus NO_x^* (ppbv) at TW during the sampling period.

ACPD
12, 29025–29067, 2012

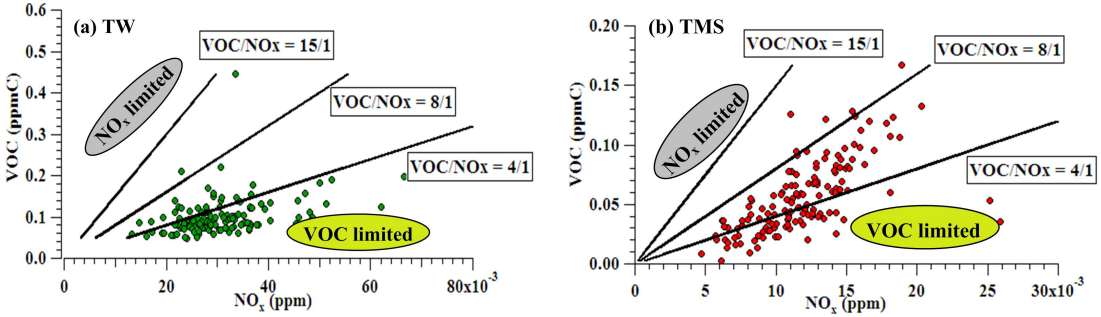

Fig. 11. Scatter plots of VOCs versus NO_x at daytime hours (07:00–18:00 LST) during sampling period at **(a)** TW and **(b)** TMS.

ACPD
12, 29025–29067, 2012

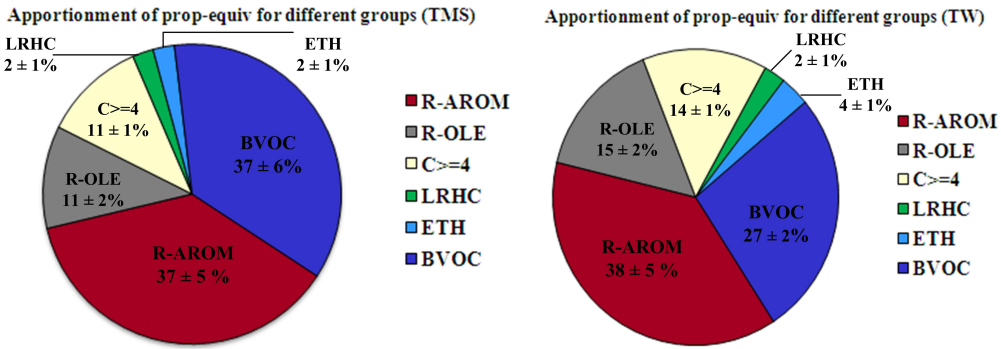

Fig. 12. Apportionment of pro-equiv for different VOC groups at TMS and TW at daytime hours (07:00–18:00 LST) during the sampling period.

ACPD
12, 29025–29067, 2012